

28 GHz Microcell Measurement Campaign for Residential Environment

C. U. Bas¹, *Student Member, IEEE*, R. Wang¹, *Student Member, IEEE*, S. Sangodoyin¹, *Student Member, IEEE*, S. Hur³, *Member, IEEE*, K. Whang³, *Member, IEEE*, J. Park³, *Member, IEEE*, J. Zhang², *Fellow, IEEE*, A. F. Molisch¹, *Fellow, IEEE*

¹University of Southern California, Los Angeles, CA, USA,

²Samsung Research America, Richardson, TX, USA

³Samsung Electronics, Suwon, Korea

Abstract—This paper presents results from the (to our knowledge) first double-directionally resolved measurement campaign at mm-wave frequencies in a suburban microcell. The measurements are performed with a real-time channel sounder equipped with phased antenna arrays that allows electrical beam steering in microseconds, and which can measure path-loss of up to 169 dB. Exploiting the phase coherency of the measurements in the different beams, we obtain both directional and omnidirectional channel power delay profiles without any delay uncertainty. We present statistics of channel characteristics such as path-loss, shadowing and delay spread results for line-of-sight and non-line-of-sight cases, as well as sample results for power angular spectrum and extracted multi-path components.

I. INTRODUCTION

Due to the ever-increasing demand for wireless data, current networks are becoming overburdened. While a variety of different techniques will be used to alleviate this congestion and enable future growth [1] [2], making new spectrum available is among the most promising approaches. For this reason, there is great interest in developing wireless communications systems in the frequency spectrum beyond 6 GHz, which up to now has been mostly fallow [3]. In a recent ruling, the frequency regulator in the USA, the Federal Communications Committee, has allowed usage of more than 10 GHz of bandwidth of that frequency range for new services - considerably more than currently used in all wireless services taken together. Other countries are expected to follow suit, and frequency bands such as 28 GHz, 38 GHz, 60 GHz and 75 GHz are being considered for fifth generation (5G) cellular networks [4]. For outdoor applications the 28 GHz currently enjoys the greatest interest, since the comparatively low frequency (compared to other mm-wave bands) allows a lower-cost implementation of many components.

The design and deployment planning of any wireless system requires a thorough understanding of the wireless propagation channel. For example, path-loss and shadowing characteristics determine distance-dependent outage probability, while delay dispersion determines spacing of subcarriers (in OFDM) or length of equalizers (in single-carrier systems). At the same time, it must be remembered that the channel characteristics strongly depend on the propagation environment. Thus, measurements of channel characteristics and creation of models

derived from them *in the environment of interest* are vital. While there have been several measurement campaigns for channel characteristics in *urban* microcellular environments (see below), to the best of our knowledge no such measurements exist in *suburban* microcell environments. The current paper aims to close this gap. In particular, we will present results from a measurement campaign in a microcellular, suburban environment with a directionally resolving, wide-band channel sounder, and extract some key channel characteristics.

Existing work: As mentioned above, a number of directionally resolved measurements have been performed in urban microcellular environments¹. The works in [5]–[7] in downtown New York City. Refs. [8] and [9] provide results in various cities in Korea, while [10] reports channel measurements conducted at 32 GHz on a University campus in Beijing, China. All these environments are densely built up, with high-rise buildings (≥ 5 floors and/or contiguous facades). All of the measurements use mechanically rotating horn antennas to extract the directional characteristics and make use of the high antenna gain to improve the link budget; the drawback of this approach is that it is very time-intensive, often requiring hours to scan a single measurement location, and thus naturally limiting the number of locations underlying the measurements.

The suburban measurements reported in the literature have been mainly focused on Fixed Wireless Access (FWA, also known as LMDS) systems [11]–[13], i.e both transmit and receive antennas are above rooftops, and thus different from the scenario considered here. Similarly, measurements in suburban environments at carrier frequencies below 6 GHz in suburban microcells exist, but due to the different frequency range cannot provide any information about mm-wave propagation.

Contributions: In this work, we present the results from the first 28 GHz channel sounding campaign in a residential suburban cellular scenario with directionally resolvable results for both TX and RX. The measurements are performed with a real-time channel sounder equipped with phased antenna arrays [14]. The phased arrays form beams at the different TX and RX angles and switch between these beams in

¹Due to space restrictions, we do not review non-directionally resolved measurement campaigns here

Table I
SOUNDER SPECIFICATIONS

Hardware Specifications	
Center Frequency	27.85 GHz
Instantaneous Bandwidth	400 MHz
Antenna array size	8 by 2 (for both TX and RX)
Horizontal beam steering	-45 to 45 degree
Horizontal 3dB beam width	12 degrees
Vertical beam steering	-30 to 30 degree
Vertical 3dB beam width	22 degrees
Horizontal/Vertical steering steps	5 degrees
Beam switching speed	2 μ s
TX EIRP	57 dBm
RX noise figure	\leq 5 dB
ADC/AWG resolution	10/15-bit
Data streaming speed	700 MBps
Sounding Waveform Specifications	
Waveform duration	2 μ s
Repetition per beam pair	10
Number of tones	801
Tone spacing	500 kHz
PAPR	0.4 dB
Total sweep time	14.44 ms



Figure 1. RX setup

microseconds, which allows measurement at a large number of locations within reasonable time, and ensures minimal variation in the environment during the performing of the measurements. We provide key channel characteristics, such as path-loss, shadowing, and delay spread, for both line-of-sight (LoS) and non-line-of-sight (NLoS) situations and present sample results for power angular spectrum and extracted multi-path components.

The rest of the paper is organized as follows. Section II discusses the channel sounder setup and the measurement environment. Section III explains the data processing. Section IV presents measurement results. Finally Section V summarizes results and suggests directions for future work.

II. MEASUREMENT CAMPAIGN

A. Channel Sounder Setup

In this campaign, we used a switched-beam, wide-band mm-wave sounder with 400 MHz real-time bandwidth [14]. The sounding signal is a multi-tone signal which consists of equally spaced 801 tones covering 400 MHz. A low peak to average power ratio (PAPR) of 0.4 dB is achieved by manipulating the phases of individual tones as suggested in [15]. This allows us to transmit with power as close as possible to the 1 dB compression point of the power amplifiers without driving them into saturation.

Both the TX and the RX have phase arrays capable of forming beams which can be electronically steered with 5° resolution in the range of $[-45^\circ, 45^\circ]$ in azimuth and $[-30^\circ, 30^\circ]$ in elevation. This decreases the measurement time for one RX location from hours to milliseconds. During this measurement campaign we only utilize a single elevation angle 0° with 19 azimuth angles both for the TX and the RX. With an averaging factor of 10, the total sweep time is 14.44 ms (without averaging it can be as low as 1.444 ms) for 361 total beam pairs. Since phased arrays cover 90° sectors, we rotated the RX to $\{0^\circ, 90^\circ, 180^\circ, 270^\circ\}$ to cover 360° while using a single orientation at the TX. Consequently, for each measurement location, we obtain a frequency response matrix of size 19 by 72 by 801. Moreover, thanks to the beam-forming gain, the TX EIRP is 57 dBm, and the measurable path loss is 159 dB without considering any averaging or processing gain. By using GPS-disciplined Rubidium frequency references, we were able to achieve both short-time and long-time phase stability. Combined with the short measurement time this limits the phase drift between TX and RX, enabling phase-coherent sounding of all beam pairs even when TX and RX are physically separated and have no cabled connection for synchronization. Consequently, the directional power delay profiles (PDP) can be combined easily to acquire the omnidirectional PDP. Table I summarizes the detailed specification of the sounder and the sounding waveform. Ref. [14] discusses further details of the sounder and the validation measurements.

B. Measurement Environment

The measurements were performed in a typical US suburban residential area at/near 28th Street in Los Angeles, CA, USA² populated with 2 to 3 story houses along a street that contains trees and other foliage, see Figure 2. Consequently, the measurements mimic a real-life cellular deployment scenario including the effect of foliage penetration loss. To imitate a microcell scenario, the TX is placed on a scissor lift at the height of 7.5 m while the RX is on a cart, and the RX antenna height is 1.8 m. The bore-sight of the 90° TX sector is parallel to the 28th St and faced towards to RX.

The RX locations are chosen for 2 different scenarios. In the first one, the RX is placed on the same street (28th St) with

²note that despite the location in Los Angeles, the building height and density is suburban, not metropolitan, as can also be seen from Figures 2,3 and 4

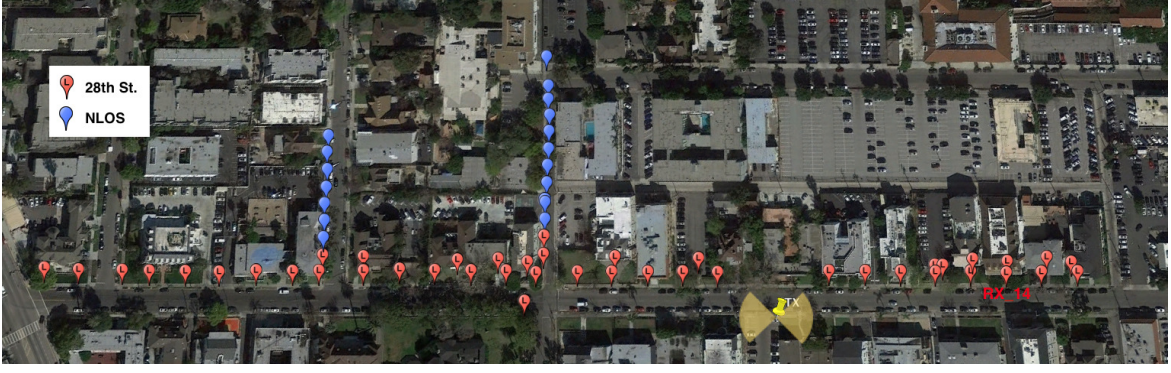


Figure 2. Measurement locations



Figure 3. RX View on 28th St facing east



Figure 4. TX View on 28th St facing west

the TX. Since in some cases the direct path is blocked by foliage or other surrounding objects, throughout the paper we call this data 28th St. instead of LOS. In the second scenario, the RX is located on the two crossing streets to create NLOS links. All RX locations are either on the sidewalks or in the front yards of the surrounding houses. The range of TX-RX separation vary from 36 m to 400 m for the 28th St and from 130 m to 273 m for NLOS.

III. DATA EVALUATIONS

The directional power delay profile (PDP) for the TX beam and RX beam with the azimuth angles θ_{TX} and θ_{RX} is estimated as;

$$P(\theta_{TX}, \theta_{RX}, \tau) = \left| \mathcal{F}^{-1} \left\{ H_{\theta_{TX}, \theta_{RX}}(\vec{f}) ./ H_{cal}(\vec{f}) \right\} \right|^2 \quad (1)$$

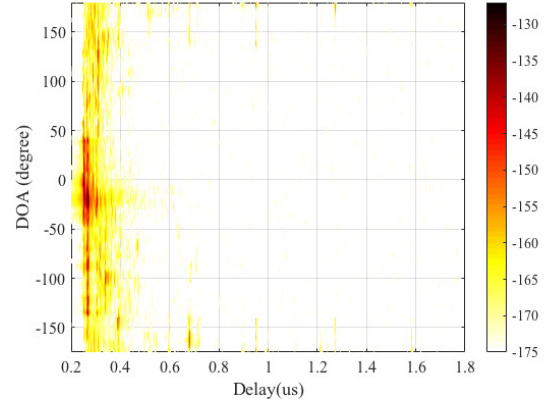


Figure 5. Power-Angular Delay Profile for RX_14

where $\theta_{RX} \in [-175, 180]$, $\theta_{TX} \in [-45, 45]$, \mathcal{F}^{-1} denotes inverse Fourier transform, $H_{\theta_{TX}, \theta_{RX}}(\vec{f})$ and $H_{cal}(\vec{f})$ are the frequency responses for TX beam θ_{TX} and RX beam θ_{RX} and, the calibration response respectively; \vec{f} are the used frequency tones, and $./$ is element-wise division.

Then the angular power spectrum can be calculated as:

$$PAS(\theta_{TX}, \theta_{RX}) = \sum_{\tau} P(\theta_{TX}, \theta_{RX}, \tau) \quad (2)$$

Figure 6 shows the $PAS(\theta_{TX}, \theta_{RX})$ for RX_14 (marked in Figure 2) along with the RX view.

Furthermore, similar to [16], the omni-directional power delay profile (PDP) power angular-delay profiles for RX and TX ($PADP_{RX/TX}$) are calculated as follows.

$$PDP(\tau) = \max_{\theta_{TX}} \max_{\theta_{RX}} P(\theta_{TX}, \theta_{RX}, \tau) \quad (3)$$

$$PADP_{RX}(\theta_{RX}, \tau) = \max_{\theta_{TX}} P(\theta_{TX}, \theta_{RX}, \tau) \quad (4)$$

$$PADP_{TX}(\theta_{TX}, \tau) = \max_{\theta_{RX}} P(\theta_{TX}, \theta_{RX}, \tau) \quad (5)$$

For the same RX location, Figures 5 and 7 show the $PADP_{RX}$ and PDP respectively. Additionally, we also consider directional PDP which is defined as the PDP acquired from the

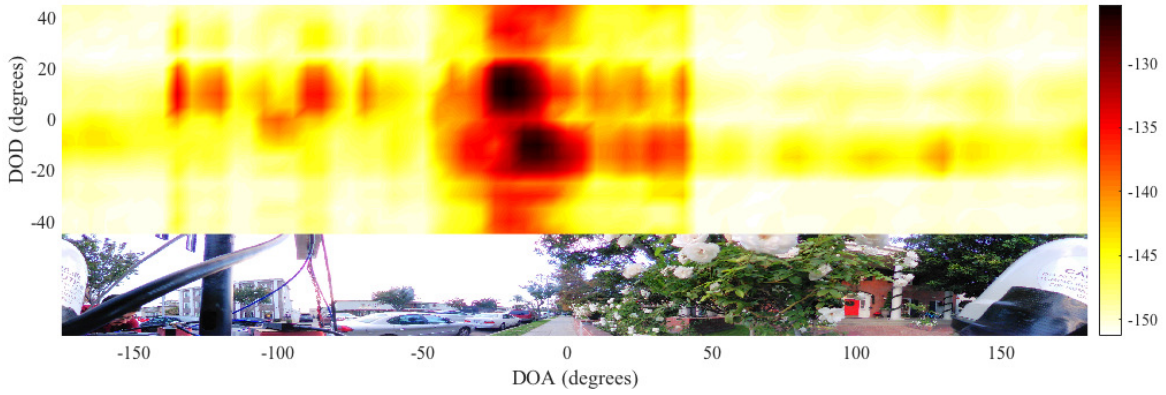


Figure 6. Power-Angular Spectrum for RX_14

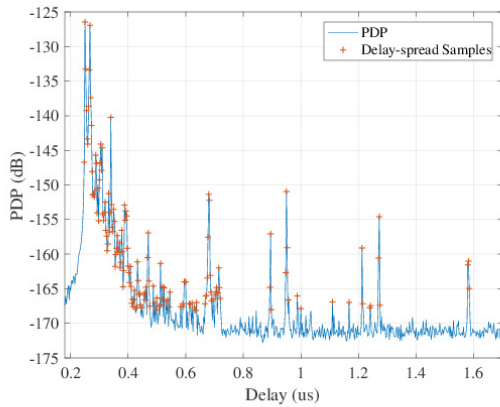


Figure 7. Power Delay Profile for RX_14

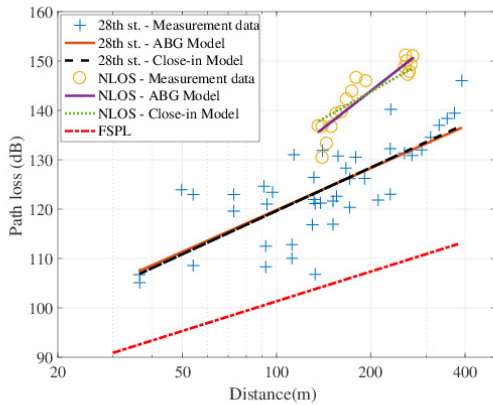


Figure 8. Path-loss for 28th St. and NLoS locations

TX-RX beam pair with the highest received power. Finally, the path-loss P_{RX} is given by:

$$P_{RX} = \sum_{\tau} PDP(\tau) \quad (6)$$

IV. RESULTS

A. Path Loss

There are two approaches commonly used for path loss modeling in mm-wave; alpha-beta-gamma (ABG) and close-in (CI) models [17] [18]. For a single frequency band, both can be simplified into:

$$PL(d) = 10n\log_{10}(d/1m) + P_0 + \chi_{\sigma} \quad (7)$$

However, they differ in the estimation of model parameters n and P_0 . For the CI method, P_0 is given by $20\log_{10}(4\pi f/c)$ which is the free-space path loss for 1m TX-RX separation at the frequency f where c is the speed of light. Once the P_0 is fixed, the path-loss exponent (PLE) n is estimated from measurement data via minimum mean square error estimation. In ABG method, both P_0 and n are estimated together from measurement data with least-squares regression. For both models χ_{σ} is a Gaussian random variable with 0 mean and standard deviation of σ in dB [17].

We used both ABG and CI models to characterize the path-loss for both omnidirectional and directional cases. Figure 8 shows the path-loss values for the 28th St and NLoS measurement points along with the ABG and CI fits for the omnidirectional RX, and the theoretical free space path-loss (FSPL). The path-loss model parameters for both directional and omnidirectional RX are given in Table II. For the 28th St, the parameters for the ABG and the CI models are very similar while they differ significantly for NLoS data. Note, however, that while the parameters are different, the resulting line fits *in the range of interest*, i.e., the range over which measurements have been made and thus the model is applicable, are quite similar. Table II also summarizes the path-loss models for the directional PDP. In the case of directional PDP, the path-loss components are slightly higher than the omnidirectional case. For 28th St, this is expected, since as the RX moves away from the probability of having an optical LoS decreases, resulting relatively higher attenuation at large distances.

For both omnidirectional scenarios, the cumulative distribution functions (CDF) of shadow fading are given in Figures 9 and 10. Both CI and ABG models follow zero-mean Gaussian

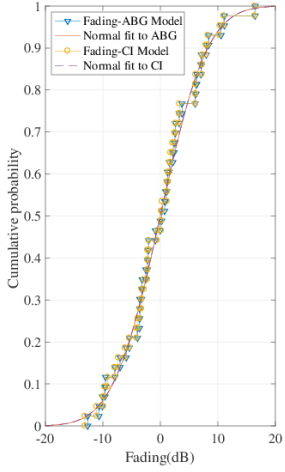


Figure 9. CDF of the fading for 28th St.

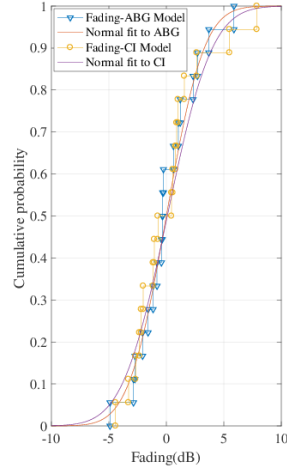


Figure 10. CDF of the fading for NLoS locations

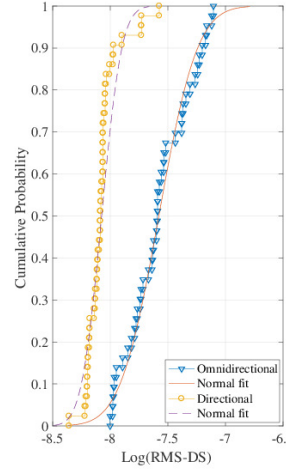


Figure 11. CDF of the logarithm of RMS-DS for 28th St.

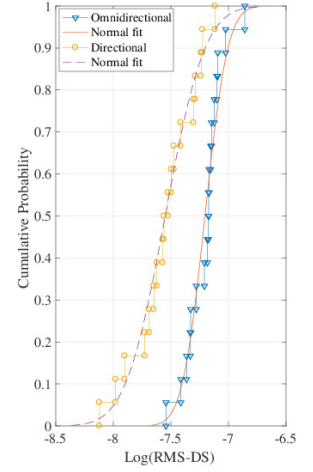


Figure 12. CDF of the logarithm of RMS-DS for NLoS locations

Table II
PARAMETERS OF THE PATH LOSS MODELS

	Data	n	P_0	χ^2	
				σ	P-value
omni	28th St - ABG Model	2.82	63.47	6.44	0.975
	28th St - CI Model	2.92	61.34	6.45	0.978
	NLoS - ABG Model	4.97	29.53	2.58	0.745
	NLoS - CI Model	3.58	61.34	3.06	0.706
directional	28th St - ABG Model	3.17	58.01	7.75	0.840
	28th St - CI Model	3.15	61.34	7.76	0.928
	NLoS - ABG Model	5.85	18.12	4.53	0.856
	NLoS - CI Model	3.96	61.34	5.06	0.958

distributions with the standard deviations listed in Table II. In 28th St, we observe a high shadow fading variance due to the foliage penetration loss and other objects along the street. Furthermore, Table II also shows the P-values of the fits, acquired via Kolmogorov-Smirnov (KS) test which uses the measure of maximum difference between the CDF of the empirical and the hypothetical distributions [19]. In all cases KS-test do not reject the hypothetical Gaussian distribution with a P-value larger than 0.7.

B. RMS Delay Spread

As is common in the literature, we characterize the delay dispersion by the root-mean-square delay spread (RMS-DS), i.e., the second central moment of the power delay profile.

$$S_\tau = \sqrt{\frac{\sum_{\hat{\tau}} PDP(\hat{\tau})\hat{\tau}^2}{P_{RX}} - \left(\frac{\sum_{\hat{\tau}} PDP(\hat{\tau})\hat{\tau}}{P_{RX}}\right)^2} \quad (8)$$

where $\{\hat{\tau} = \tau | PDP(\tau) > 2\sigma_{noise}^2\}$ and σ_{noise}^2 is the noise power for omnidirectional PDP.

Prior to the RMS-DS calculation, we apply noise filtering to avoid any contribution of the noise floor, which can significantly distort delay spread calculations by creating nonphysical contributions at large delays. Due to the automatic gain control implemented at the RX, the noise level might vary

between directional PDPs for different beam pairs. Hence, we first obtain noise-filtered directional PDPs by:

$$P(\theta_{TX}, \theta_{RX}, \tau) = \begin{cases} P(\theta_{TX}, \theta_{RX}, \tau) & \text{if } P(\theta_{TX}, \theta_{RX}, \tau) > 4\sigma^2(\theta_{TX}, \theta_{RX}) \\ 0 & \text{otherwise} \end{cases} \quad (9)$$

where $\sigma^2(\theta_{TX}, \theta_{RX})$ is the noise power for TX beam θ_{TX} and RX beam θ_{RX} . Figure 5 shows the noise-filtered $PADP_{RX}$ for RX_14. Then the omnidirectional PDP is calculated by using Equation 3.

A sample omnidirectional PDP and the samples used for delay spread calculation are shown in Figure 7. Figure 11 and 12 show the cumulative distribution functions of the Log(RMS-DS) along with the corresponding Gaussian fits for 28th St and NLoS, respectively. As listed in Table III, the median RMS-DS are 25.63 ns for 28th St. and 67.18 ns for NLoS. The mean μ of the Gaussian fits are -7.58 for 28th St and -7.2 for NLoS. In [20], for urban-micro scenario, they modeled the μ of the Log(RMS-DS) as $\mu = -0.2 \text{Log}(1+f) - 7.2$ and $\mu = -0.21 \text{Log}(1+f) - 6.88$ for LOS and NLoS respectively. At 27.85 GHz, the corresponding μ values are -7.49 and -7.19 which are well-aligned with our results. We also investigate the delay spread values for the directional case, i.e., for the TX/RX beam combination that provides that highest receive power. In case of LOS 86% of the links have RMS-DS within 5 ns to 10 ns, see Figure 11, and the median is 8.7 ns. For NLoS, the directional RMS-DS vary from 8 ns to 70 ns as seen in Figure 12. We thus see that the ratio of omni-directional to directional delay spread is on the order of 3, a result that is comparable to the results in [5] for urban environments.

C. Extracted Multi-paths

By performing 3-dimensional peak detection in the $P(\theta_{TX}, \theta_{RX}, \tau)$ we extract the multi-path components (MPC) with the information of; direction of departure (DOD), direction of arrival (DOA), delay and path gain. To avoid the ghost paths due to sidelobes of the beams, for every delay bin, we

Table III
PARAMETERS OF THE RMS-DS

	Median(ns)	μ	σ	P-value
28th St - omni	25.63	-7.58	0.263	0.889
28th St - directional	8.19	-8.10	0.101	0.254
NLoS - omni	67.18	-7.20	0.156	0.664
NLoS - directional	28.71	-7.55	0.271	0.991

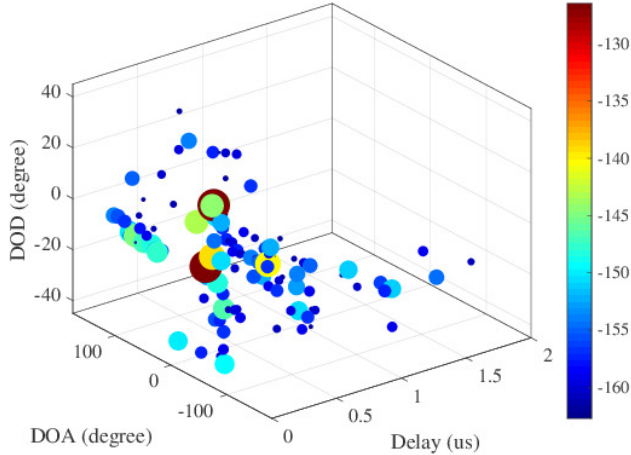


Figure 13. Extracted multi-path components

filter out any MPCs with 10 dB or less path gain compared to the highest power MPC in the same delay bin. The extracted MPCs for the RX₁₄ are shown in Figure 13.

V. CONCLUSION

In this paper we presented results from a channel sounding campaign in a residential suburban environment at 28 GHz. The novel design of the channel sounder allowed phase-coherent measurements of all TX and RX angles. For path-loss, we provided parameters for both ABG and CI models. Although the environment is not urban, we saw that the mean RMS-DS results are inline with the Urban micro-cellular model provided in [20]. We showed that the channel sounder used in this campaign is capable of angular investigations for both TX and RX. In the future, we will provide statistics for angular spreads, perform more measurement campaigns to investigate the outdoor-to-indoor penetration loss and foliage effects.

ACKNOWLEDGEMENT

Part of this work was supported by grants from the National Science Foundation. The authors would like to thank Sundar Aditya, Vinod Kristem, He Zeng for efforts in helping the measurement campaign and Dimitris Psychoudakis, Thomas Henige, Robert Monroe for their contribution in the development of the channel sounder.

REFERENCES

[1] N. Al-Falahy and O. Y. Alani, "Technologies for 5G Networks: Challenges and Opportunities," *IT Professional*, vol. 19, no. 1, pp. 12–20, Jan 2017.

[2] J. G. Andrews, S. Buzzi, W. Choi, S. V. Hanly, A. Lozano, A. C. Soong, and J. C. Zhang, "What will 5g be?" *Selected Areas in Communications, IEEE Journal on*, vol. 32, no. 6, pp. 1065–1082, 2014.

[3] F. Boccardi, R. W. Heath, A. Lozano, T. L. Marzetta, and P. Popovski, "Five disruptive technology directions for 5G," *IEEE Communications Magazine*, vol. 52, no. 2, pp. 74–80, February 2014.

[4] F. C. Commission *et al.*, "In the matter of use of spectrum bands above 24 GHz for mobile radio services," *Notice of Proposed Rulemaking in FCC*, pp. 15–138, 2015.

[5] T. Rappaport, G. Maccartney, M. Samimi, and S. Sun, "Wideband millimeter-wave propagation measurements and channel models for future wireless communication system design," *Communications, IEEE Transactions on*, vol. 63, no. 9, pp. 3029–3056, Sept 2015.

[6] G. R. MacCartney, M. K. Samimi, and T. S. Rappaport, "Omnidirectional path loss models in New York City at 28 GHz and 73 GHz," in *Personal, Indoor, and Mobile Radio Communication (PIMRC), 2014 IEEE 25th Annual International Symposium on*. IEEE, 2014, pp. 227–231.

[7] A. I. Sulyman, A. T. Nassar, M. K. Samimi, G. R. Maccartney, T. S. Rappaport, and A. Alsanie, "Radio propagation path loss models for 5G cellular networks in the 28 GHz and 38 GHz millimeter-wave bands," *IEEE Communications Magazine*, vol. 52, no. 9, pp. 78–86, 2014.

[8] J.-J. Park, J. Liang, J. Lee, H.-K. Kwon, M.-D. Kim, and B. Park, "Millimeter-wave channel model parameters for urban microcellular environment based on 28 and 38 GHz measurements," in *Personal, Indoor, and Mobile Radio Communications (PIMRC), 2016 IEEE 27th Annual International Symposium on*. IEEE, 2016, pp. 1–5.

[9] S. Hur, S. Baek, B. Kim, J. Park, A. Molisch, K. Haneda, and M. Peter, "28 ghz channel modeling using 3d ray-tracing in urban environments," in *Antennas and Propagation (EuCAP), 2015 9th European Conference on*, April 2015, pp. 1–5.

[10] X. Zhao, S. Li, Q. Wang, M. Wang, S. Sun, and W. Hong, "Channel measurements, modeling, simulation and validation at 32 GHz in outdoor microcells for 5G radio systems," *IEEE Access*, vol. 5, pp. 1062–1072, 2017.

[11] P. B. Papazian, G. A. Hufford, R. J. Achatz, and R. Hoffman, "Study of the local multipoint distribution service radio channel," *IEEE Transactions on Broadcasting*, vol. 43, no. 2, pp. 175–184, Jun 1997.

[12] Z. Muhi-Eldeen, L. P. Ivrisimtzis, and M. Al-Nuaimi, "Modelling and measurements of millimetre wavelength propagation in urban environments," *IET Microwaves, Antennas Propagation*, vol. 4, no. 9, pp. 1300–1309, September 2010.

[13] H. Xu, T. S. Rappaport, R. J. Boyle, and J. H. Schaffner, "Measurements and models for 38-GHz point-to-multipoint radiowave propagation," *IEEE Journal on Selected Areas in Communications*, vol. 18, no. 3, pp. 310–321, March 2000.

[14] C. U. Bas, R. Wang, D. Psychoudakis, T. Henige, R. Monroe, J. Park, J. Zhang, and A. F. Molisch, "A Real-Time Millimeter-Wave Phased Array MIMO Channel Sounder," *arXiv preprint arXiv:1703.05271*, 2017.

[15] M. Friese, "Multitone signals with low crest factor," *Communications, IEEE Transactions on*, vol. 45, no. 10, pp. 1338–1344, 1997.

[16] S. Hur, Y. J. Cho, J. Lee, N.-G. Kang, J. Park, and H. Benn, "Synchronous channel sounder using horn antenna and indoor measurements on 28 ghz," in *2014 IEEE International Black Sea Conference on Communications and Networking (BlackSeaCom)*, May 2014, pp. 83–87.

[17] T. S. Rappaport, G. R. MacCartney, M. K. Samimi, and S. Sun, "Wideband millimeter-wave propagation measurements and channel models for future wireless communication system design," *IEEE Transactions on Communications*, vol. 63, no. 9, pp. 3029–3056, Sept 2015.

[18] A. F. Molisch, A. Karttunen, R. Wang, C. U. Bas, S. Hur, J. Park, and J. Zhang, "Millimeter-wave channels in urban environments," in *2016 10th European Conference on Antennas and Propagation (EuCAP)*, April 2016, pp. 1–5.

[19] F. J. Massey Jr, "The Kolmogorov-Smirnov test for goodness of fit," *Journal of the American statistical Association*, vol. 46, no. 253, pp. 68–78, 1951.

[20] "5G Channel Model for bands up to 100 GHz," Aalto University, AT&T, BUPT, CMCC Ericsson Huawei, INTEL, KT Corporation, Nokia, NTT DOCOMO, New York University, Qualcomm, Samsung, University of Bristol, University of Southern California, Tech. Rep., 04 2016.